IEEE Access
Multidisciplinary | Rapid Review | Open Access Journal

Received October 26, 2018, accepted November 8, 2018, date of publication November 13, 2018,
date of current version December 31, 2018.

Digital Object Identifier 10.1109/ACCESS.2018.2881133

Performance Comparison of Model Predictive Control Methods for Active Front End Rectifiers

EUN-SU JUN[1], SANGSHIN KWAK[1], (Member, IEEE), AND TAEHYUNG KIM[2], (Senior Member, IEEE)

[1]School of Electrical and Electronics Engineering, Chung-Ang University, Seoul 156-756, South Korea
[2]Department of Electrical and Computer Engineering, University of Michigan–Dearborn, Dearborn, MI 48128, USA

Corresponding author: Sangshin Kwak (sskwak@cau.ac.kr)

This work was supported in part by the National Research Foundation of Korea (NRF), a grant funded by the Korean Government (MSIP), under Grant 2017R1A2B4011444 and in part by the Chung-Ang University Graduate Research Scholarship in 2018.

ABSTRACT Active front-end rectifiers are tasked with generating high-quality, low-distortion sinusoidal line currents in the presence of adverse circuit conditions. When suitable control methods are applied to such rectifiers, significant performance improvements can be realized, especially under abnormal utility conditions. Although several control methods based on model predictive control platforms have been recently developed, there is a lack of comparative studies of these methods in the literature. In this paper, the details and theoretical background of four model predictive control methods, namely, current control, virtual flux control, direct power control, and virtual flux direct power control, are presented. Then, the performance of these methods was compared by the way of experiments to determine the respective quality of the line current under various conditions, such as unbalanced input voltages, input voltage distortion, uncertainty in the parameters, and dc voltage fluctuation. In summary, based on the results of the experiments, the virtual flux control scheme was found to be distinctly superior to the other three schemes for distorted and unbalanced line voltages.

INDEX TERMS Active front end rectifier, current control, direct power control, model predictive control, virtual flux control.

I. INTRODUCTION

The recently growing need to synthesize sinusoidal line currents with low distortion under adverse conditions requires active front end (AFE) rectifiers instead of diode rectifiers as they provide high quality line currents with low total harmonic distortion (THD), adjustable output voltages, unity power factors, and regenerative capability [1].

Several AFE rectifier control methods have been proposed in the literature [2], [3], including voltage-oriented control (VOC) and direct power control (DPC) schemes [4]–[6], that enable the generation of sinusoidal line currents even when the input line voltages are abnormal. More recently, finite control-set model predictive control methods have been proposed for these applications [7]–[9] that predict the values of the control variables at the next step in order to determine the optimal switching state. These predictive control methods are appealing due to their advantages, such as a fast dynamic response, a simple structure that does not include a pulse width modulation block, and the ability to easily include constraints. These methods have also benefitted from ongoing developments in high speed, cost-effective microprocessors [10]–[12]. There are four possible AFE rectifier control methods that are applicable to finite control-set model predictive control algorithms: model predictive current control (MP-CC), model predictive virtual flux control (MP-VFC), model predictive direct power control (MP-DPC), and model predictive virtual flux direct power control (MP-VFDPC). All of these methods are based on a common predictive control method, which includes predicting the future behavior of the control variables and evaluating a cost function. Here, the cost function compares the reference value of a control variable with all possible predicted future values of a corresponding set of control variables. Although the four methods are based on the same control principle, the respective performance of AFE rectifiers controlled by each of the methods differ depending on the control variables employed in the controllers. The MP-CC algorithm [10], [13], [14] directly controls the line currents of the AFE rectifier by employing the line current itself as a control variable, whereas the MP-VFC method [15], [16] utilizes the virtual fluxes of the rectifier input voltages as a control target. By contrast, the MP-DPC [17], [18]

and MP-VFDPC methods [19]–[22] adjust the input real and reactive power components of the AFE rectifier based on the power elements as a control target. Although these last two schemes both utilize the real and reactive power components as control targets, they adopt different approaches to calculate the future power elements at the next step.

The objective of this paper is to discuss and compare the features and performance of the four listed model predictive control methods. First, the theoretical background for these methods is presented. Then, experimental results are used to develop a detailed comparison of the rectifiers in terms of their line current qualities under various conditions, such as an unbalanced input voltage, input voltage distortion, parametric uncertainty, and dc voltage fluctuation. Finally, the conclusions that can be drawn from this research are presented.

II. THEORETICAL BACKGROUD FOR FOUR MODEL PREDICTIVE CONTROL METHODS FOR ACTIVE FRONT END RECTIFIERS

The topology of an AFE rectifier is depicted in Fig. 1, where $\mathbf{v}_s$ is the input phase voltage, R is the line resistance, L is the line inductance, $\mathbf{i}_{line}$ is the line current, $\mathbf{v}_{con}$ is the rectifier input voltage, and V_{dc} is the output voltage of the rectifier.

Fig. 2 represents the MP-CC control block, in which the line currents of the AFE rectifier are directly controlled because they are employed as a control variable in the control platform. Thus, future behaviors of the line currents are predicted based on the rectifier dynamic equations and a cost function is designed to force the line currents to track the references. The dynamic equation, set up at the rectifier input terminals and expressed in a discrete time domain, is [10], [13]

$$\mathbf{i}_{line}(k+1) = \left(1 - \frac{RT_s}{L}\right)\mathbf{i}_{line}(k) + \frac{T_s}{L}\left(\mathbf{v}_s(k) - \mathbf{v}_{con}(k)\right), \tag{1}$$

where $\mathbf{i}_{line}(k+1)$ represents the future values of the line currents at the $(k+1)^{\text{th}}$ step and T_s is the sampling period. In addition, $\mathbf{i}_{line}(k)$, $\mathbf{v}_s(k)$, and $\mathbf{v}_{con}(k)$ represent the present values of the line currents, line voltages, and AFE input voltages, respectively. Because the rectifier input voltage $\mathbf{v}_{con}(k)$ is determined by the switching states of the AFE rectifier, seven future values of the $\mathbf{i}_{line}(k+1)$ based on the next step switching states can be obtained via (1). By comparing the seven predicted line current values with the future value of the line current reference as per the cost function in (2), the optimal switching state at the next step can be determined.

$$g_{MP-CC} = \left|\mathbf{i}^*_{line}(k+1) - \mathbf{i}_{line}(k+1)\right|. \tag{2}$$

The magnitude of the line current reference is produced by the proportional and integral (PI) controller to regulate the output voltage of the AFE rectifier and the phase of the current reference is taken by the line voltage phase for unity power factor operation as shown in Fig. 2. By choosing the next switching command so as to minimize the cost function, the line current at the next step tracks the line current reference. Note that the well-known delay compensation algorithm that is commonly used to compensate for the one-step delay that occurs in practical controllers is not included in this section for the four control methods in theory [14].

A schematic of an MP-VFC control block is shown in Fig. 3. The MP-VFC method employs the virtual flux,

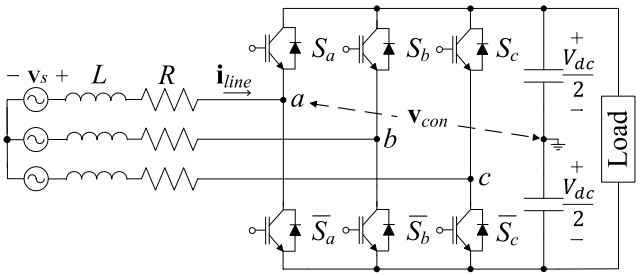

FIGURE 1. AFE rectifier.

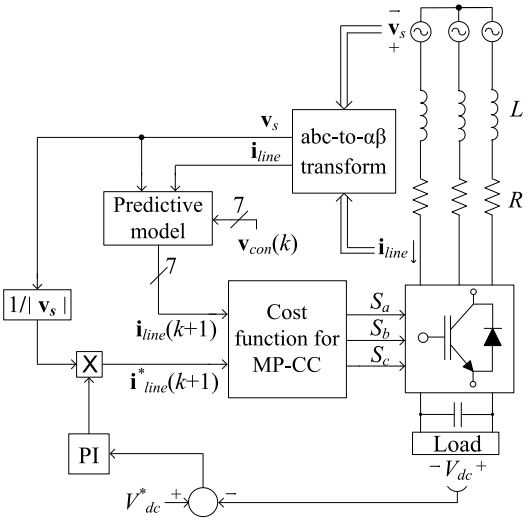

FIGURE 2. Control block for the model predictive current control (MP-CC) scheme.

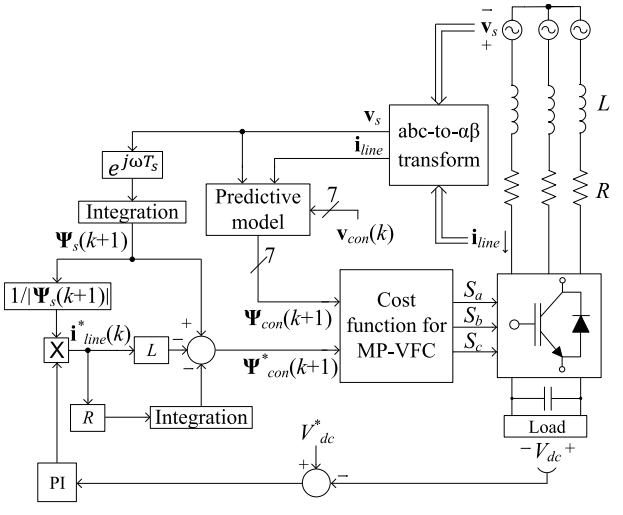

FIGURE 3. Control block for the model predictive virtual flux control (MP-VFC) scheme.

which is resistant to distortions in the input voltage, as a control variable to operate the AFE rectifiers, whereas the MP-CC method uses the input voltage itself for AFE rectifier control. This former method calculates the future values of the rectifier virtual flux $\boldsymbol{\psi}_{con}(k+1)$ based on the line current and AFE input voltage using Euler's backward approximation for discretization, as shown in (3) [15], [16].

$$\begin{aligned}\boldsymbol{\psi}_{con}(k+1) = \boldsymbol{\psi}_{s}(k+1) - \sum_{n=0}^{n=k} R\mathbf{i}_{line}(n)\,T_s \\ - L(1+\frac{RT_s}{L})\{\left(1-\frac{RT_s}{L}\right)\mathbf{i}_{line}(k) \\ + \frac{T_s}{L}(\mathbf{v}_s(k) - \mathbf{v}_{con}(k))\},\end{aligned} \tag{3}$$

where $\boldsymbol{\psi}_{s}(k+1) = \sum_{n=0}^{n=k}\mathbf{v}_s(n)T_s + \mathbf{v}_s(k+1)T_s$ and $\mathbf{v}_s(k+1) = \mathbf{v}_s(k)e^{j\omega T_s}$. Similarly, the future virtual flux reference of the AFE rectifier $\boldsymbol{\psi}^*_{con}(k+1)$ can also be obtained together with the line voltages and the PI controller for regulating the output voltage of the AFE rectifier as:

$$\begin{aligned}\boldsymbol{\psi}^*_{con}(k+1) = \boldsymbol{\psi}_{s}(k+1) - L\mathbf{i}^*_{line}(k+1) \\ - \sum_{n=0}^{n=k+1} R\mathbf{i}^*_{line}(n)\,T_s.\end{aligned} \tag{4}$$

The cost function in (5) is used to evaluate seven possible future virtual flux values in comparison to the reference virtual flux in order to select an optimal switching state.

$$g_{MP-VFC} = \left|\boldsymbol{\psi}^*_{con}(k+1) - \boldsymbol{\psi}_{con}(k+1)\right|. \tag{5}$$

The model predictive direct power control (MP-DPC) method directly adjusts the input power components of the AFE rectifier, by using the real and the reactive power elements, P and Q, respectively, as control variables for the model predictive control algorithm. The future instantaneous input powers are predicted using the line voltages and line currents predicted in (1) as follows [17], [18]:

$$\begin{aligned}P(k+1) = \mathrm{v}_{s\alpha}(k+1)\,\mathrm{i}_{line\alpha}(k+1) \\ + \mathrm{v}_{s\beta}(k+1)\,\mathrm{i}_{line\beta}(k+1),\end{aligned} \tag{6}$$

$$\begin{aligned}Q(k+1) = \mathrm{v}_{s\beta}(k+1)\,\mathrm{i}_{line\alpha}(k+1) \\ - \mathrm{v}_{s\alpha}(k+1)\,\mathrm{i}_{line\beta}(k+1),\end{aligned} \tag{7}$$

where $\mathbf{i}_{line} = \mathrm{i}_{line\alpha} + j\mathrm{i}_{line\beta}$ and $\mathbf{v}_s = \mathrm{v}_{s\alpha} + j\mathrm{v}_{s\beta}$. In the MP-DPC algorithm, the reference real power P^* is obtained as the output of the PI controller used to regulate the dc output voltage of the AFE rectifier. On the other hand, the reference reactive power Q^* is generally set to zero for unity power factor operation. Among the eight possible switching states which produce the seven voltage vectors due to zero vector obtained by two zero switching states, one optimal switching state corresponding to an optimal rectifier input voltage vector is selected to minimize the input power error based on a cost function, which is defined as follows [24], [25]:

$$g_{MP-DPC} = |P^*(k+1) - P(k+1)| + |Q^*(k+1) - Q(k+1)| \tag{8}$$

As was the case for the MP-DPC scheme, the real and the reactive power components are employed as control variables in the MP-VFDPC method. Similarly, the cost function in (8) for the MP-DPC method is also used for the MP-VFDPC method. However, the two methods differ in their approach to calculating the future power components. The MP-DPC algorithm predicts the line currents and line voltages in order to obtain the future power component values, whereas to minimize the adverse effects of harmonic distortion of the line voltages, the MP-VFDPC method calculates the future power by predicting the next-step line current and the next-step virtual flux as per (9) and (10) [19], [23], [26]:

$$\begin{aligned}P(k+1) = \omega(\psi_{s\alpha}(k+1)\,\mathrm{i}_{line\beta}(k+1) \\ - \psi_{s\beta}(k+1)\,\mathrm{i}_{line\alpha}(k+1)),\end{aligned} \tag{9}$$

$$\begin{aligned}Q(k+1) = \omega(\psi_{s\alpha}(k+1)\,\mathrm{i}_{line\alpha}(k+1) \\ + \psi_{s\beta}(k+1)\,\mathrm{i}_{line\beta}(k+1)),\end{aligned} \tag{10}$$

where,

$$\begin{aligned}\mathrm{i}_{line\alpha}(k+1) = \left(1-\frac{RT_s}{L}\right)\mathrm{i}_{line\alpha}(k) \\ + \frac{T_s}{L}\left(-\omega\psi_{s\beta}(k) - \mathrm{v}_{con\alpha}(k)\right),\end{aligned}$$

$$\begin{aligned}\mathrm{i}_{line\beta}(k+1) = \left(1-\frac{RT_s}{L}\right)\mathrm{i}_{line\beta}(k) \\ + \frac{T_s}{L}\left(\omega\psi_{s\alpha}(k) - \mathrm{v}_{con\beta}(k)\right),\end{aligned}$$

$\boldsymbol{\psi}_s = \psi_{s\alpha} + j\psi_{s\beta}$, $\mathbf{v}_{con} = \mathrm{v}_{con\alpha} + j\mathrm{v}_{con\beta}$, and ω is the angular frequency of the line voltage.

III. COMPARISONS OF THE FOUR CONTROL METHODS

In this section, a comparison of the performance of each of the four control methods is provided. To ensure an unbiased comparison, the following parameters and constraints were applied to all methods:

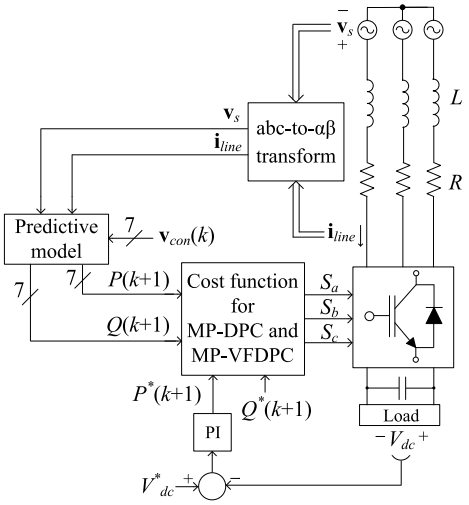

FIGURE 4. Control block for the model predictive virtual flux (MP-DPC) scheme.

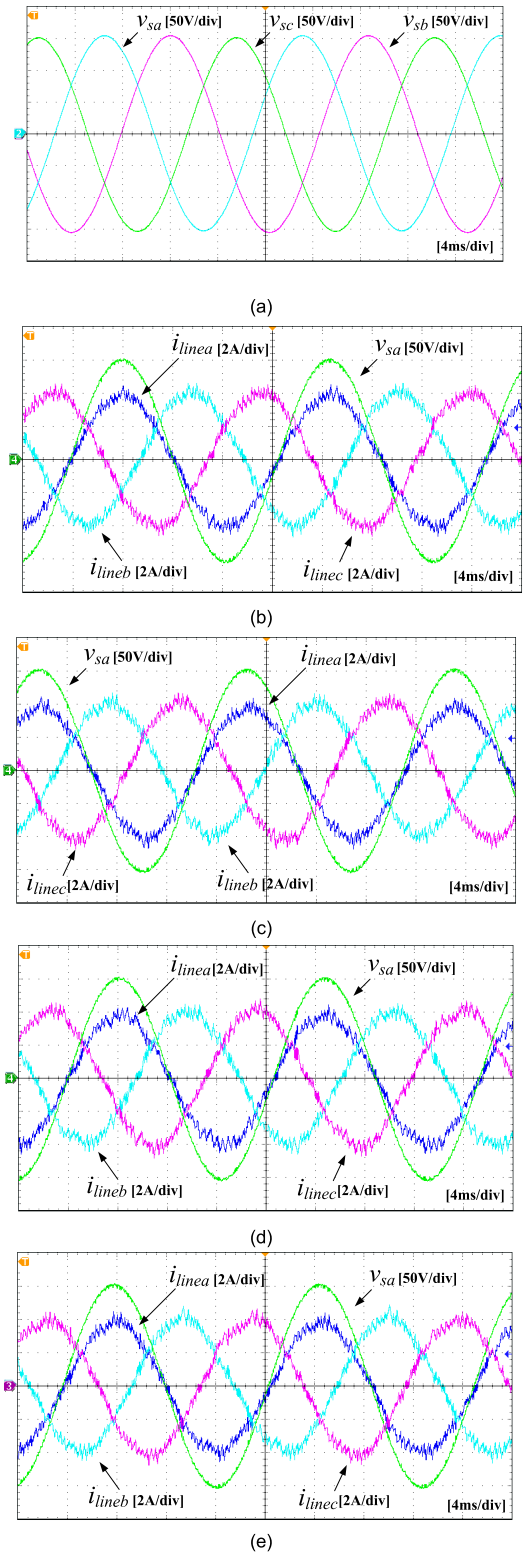

FIGURE 5. Experimental waveforms of the three-phase rectifier input currents with no line voltage distortion obtained with (a) three-phase line voltages (b) MPCC method (c) MP-VFC method (d) MP-DPC method, and (e) MP-VFDPC method.

1) *Unity power factor operation with 110 V input supply phase voltage (rms) and 60 Hz frequency*
2) *10 mH input filter inductance, 1 Ω input filter resistance, 1.1 mF output filter capacitance, and 100 Ω load resistance*
3) *20 kHz sampling frequency*

In addition, the reference dc voltage is set to 300 V. The comparison was conducted for line voltages distorted by the addition of 5th and 7th harmonics and unbalanced line voltages. The performance of each method was then evaluated based on its robustness to parameter uncertainties, the calculation complexity, and the dynamic speed under transient conditions. For comparison purposes, a three-phase AFE rectifier was constructed in a laboratory and the four control methods were implemented on a Texas Instruments DSP board (TMS320F28335). Fig. 5 illustrates the experimental results of the line current waveforms obtained by the four control methods with balanced supply voltages with no distortion as shown in Fig. 5 (a). It is seen from Fig. 5 that the four control methods generate sinusoidal line current waveforms that are in phase with the line voltages.

A. EFFECT OF THE DISTORTED LINE VOLTAGES

Fig. 6 shows the average THD values of the line currents resulting from the four control methods with distorted line voltages. Because the 5th and the 7th harmonic components are most dominant components in three-phase power supplies, their effects on AFE rectifier performances are investigated in this paper. The applied distortion was as follows. The a-phase line voltage was contaminated by the addition of the 5th harmonic component while no harmonic components were added to the b- and c-phases. This can be mathematically described as follows [12], [27], [28].

$$\begin{aligned} \mu v_{sa} &= V_m \sin(\omega t) + {}_{a5}V_m \sin(5\omega t) \\ \mu v_{sb} &= V_m \sin\left(\omega t - \frac{2}{3}\pi\right) + {}_{b5}V_m \sin\left(5\omega t + \frac{2}{3}\pi\right) \\ \mu v_{sc} &= V_m \sin\left(\omega t + \frac{2}{3}\pi\right) + {}_{c5}V_m \sin\left(5\omega t - \frac{2}{3}\pi\right), \end{aligned} \quad (11)$$

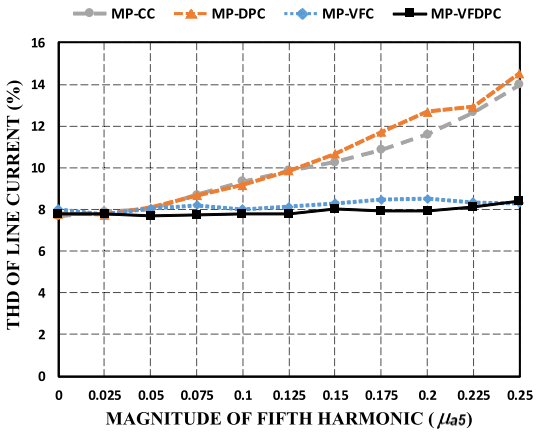

FIGURE 6. Average THD values of line currents resulting from four control methods under distorted line voltage with a-phase line voltage contaminated with 5th harmonics (μ_{a5} varying from zero to 0.25, $\mu_{b5} = 0$ and $\mu_{c5} = 0$).

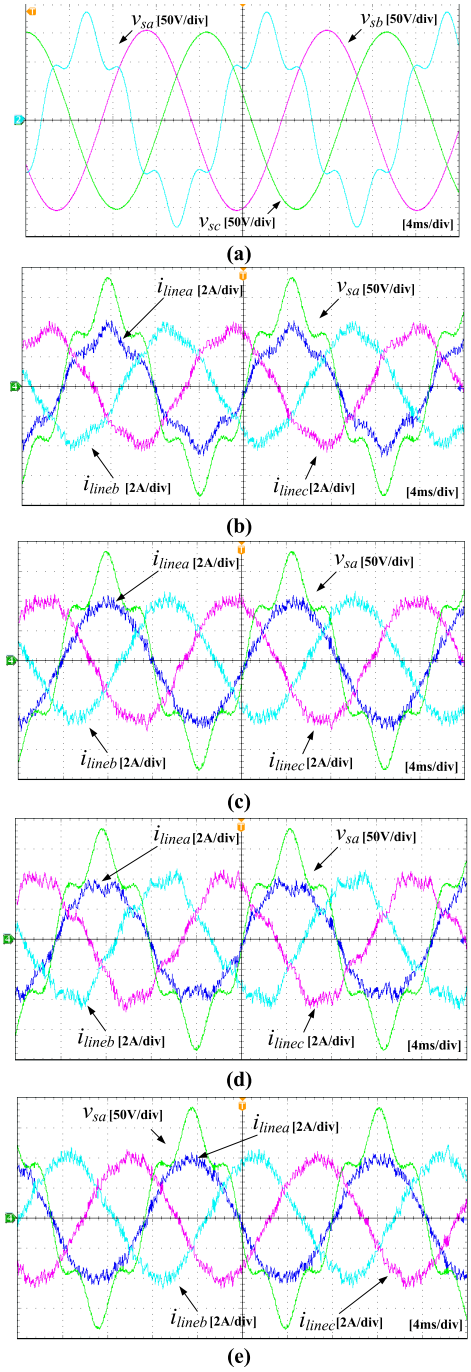

FIGURE 7. Experimental waveforms of three-phase line currents under distorted line voltage with *a*-phase source contaminated with 5th harmonics by 20 percent ($\mu_{a5} = 0.2$, $\mu_{b5} = 0$ and $\mu_{c5} = 0$) with (a) three-phase line voltages (b) MPCC method (c) MP-VFC method (d) MP-DPC method, and (e) MP-VFDPC method.

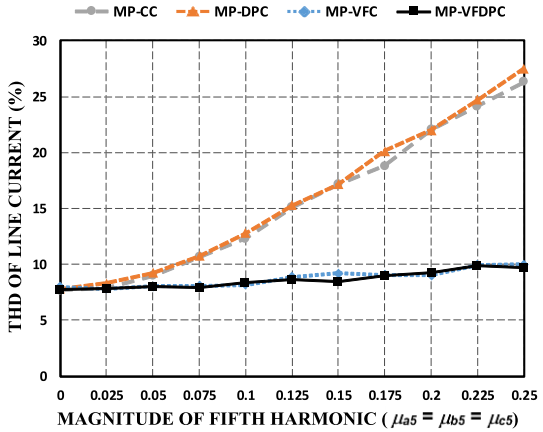

FIGURE 8. Average THD values of line currents resulting from four control methods under distorted line voltage with three-phase sources contaminated with 5th harmonics ($\mu_{a5} = \mu_{b5} = \mu_{c5}$, which vary from zero to 0.25).

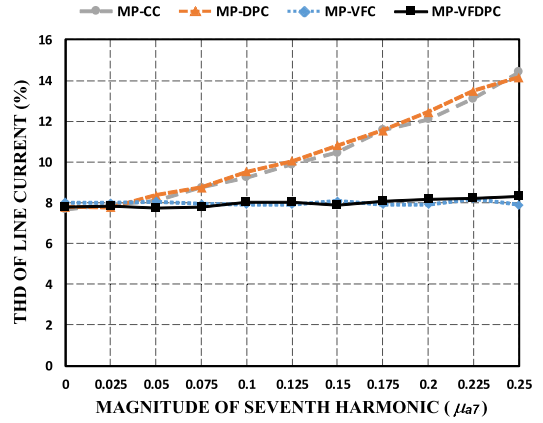

FIGURE 9. Average THD values of line currents resulting from four control methods under distorted line voltage with *a*-phase source contaminated with 7th harmonics (μ_{a7} varying from zero to 0.25, $\mu_{b7} = 0$ and $\mu_{c7} = 0$).

where, V_m represents the magnitude of the fundamental component of the line voltages and $\mu_{i5}(i = a, b, c)$ represents the ratio between the magnitude of the 5th harmonic and the magnitude of the fundamental component for each phase of the line voltages. The THD values of the line currents in Fig. 6 were computed by inputting the measured line current data into the power analysis application module in the Tektronix digital oscilloscope (500 MHz MSO3054) used in the experiments. The power analysis module was configured to evaluate the components up to the 80th harmonic while ignoring the inter-harmonic components. The following equation was used to calculate the average THD values:

$$\mathrm{THD} = \frac{\mathrm{THD_a} + \mathrm{THD_b} + \mathrm{THD_c}}{3}. \tag{12}$$

where,

$$\mathrm{THD}_i = \frac{\sqrt{I_{irms}^2 - I_{i1,rms}^2}}{I_{i1,rms}^2} \quad (i = a, b, c)$$

It can be seen in Fig. 6 that the four control methods produced almost the same supply current THDs with no 5th harmonic distortion. However, as the magnitude of μ_{a5} increased, the average THD values also increased. The MP-CC and MP-DPC methods produced increasing THD values in proportion to the increasing magnitude of the

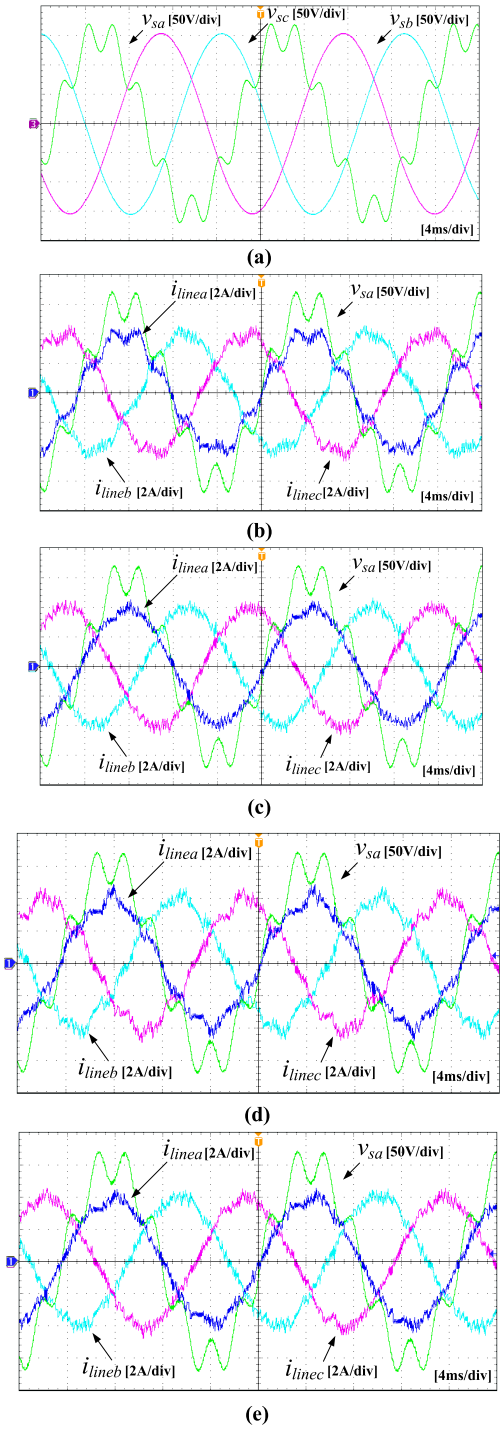

FIGURE 10. Experimental waveforms of three-phase line currents under the distorted supply voltage with *a*-phase source contaminated with 7^{th} harmonics ($\mu_{a7} = 0.2$, $\mu_{b7} = 0$ and $\mu_{c7} = 0$) with (a) three-phase line voltage (b) MP-CC method (c) MP-VFC method (d) MP-DPC method, and (e) MP-VFDPC method.

5^{th} harmonic component of the *a*-phase line voltage. In contrast, the MP-VFC and MP-VFDPC methods were found to be less sensitive to the 5^{th} harmonic distortion of the *a*-phase supply voltage due to its reliance on the virtual flux effects.

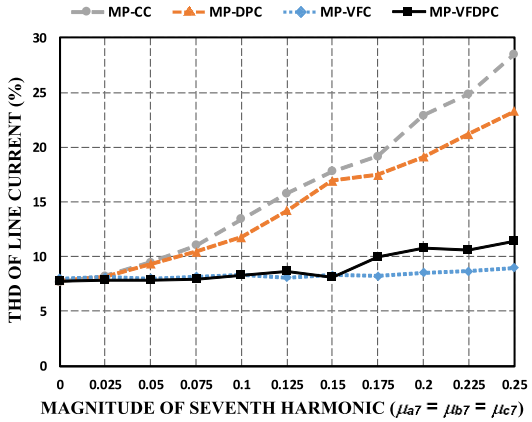

FIGURE 11. Average THD values of line currents resulting from four control methods under distorted line voltage with three-phase source contaminated with 7^{th} harmonics ($\mu_{a7} = \mu_{b7} = \mu_{c7}$, which vary from zero to 0.25).

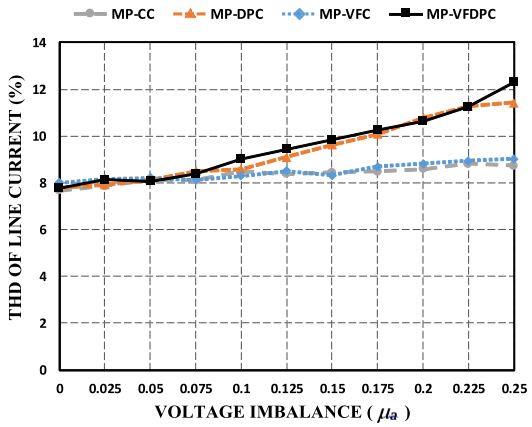

FIGURE 12. Average THD values of line currents resulting from four control methods under line voltage imbalance with *a*-phase source unbalanced (μ_a varying from zero to 0.25, $\mu_b = 0$, and $\mu_c = 0$).

The experimental results of the three-phase line current waveforms obtained via the four control methods for a distorted line voltage are shown in Fig. 7. In this case, the *a*-phase source was contaminated by the addition of a 20% ($\mu_{a5} = 0.2$)5^{th} harmonic component, which was obtained by a programmable AC power source (Chroma programmable AC source model 61702). The combined waveform is shown in Fig. 7 (a). As illustrated by the remaining subfigures, the four control methods generated *a*-phase input currents that were in-phase with the *a*-phase line voltage regardless of the magnitude of the distortion of the *a*-phase line voltage. However, unlike the displacement power factor, the line current waveforms and harmonic components contained in the currents differed depending on the respective control method. In the figure, it can be seen that the MP-VFC and MP-VFDPC methods resulted in current waveforms that were less contaminated and had better harmonic performance than those of the MP-CC and the MP-DPC methods.

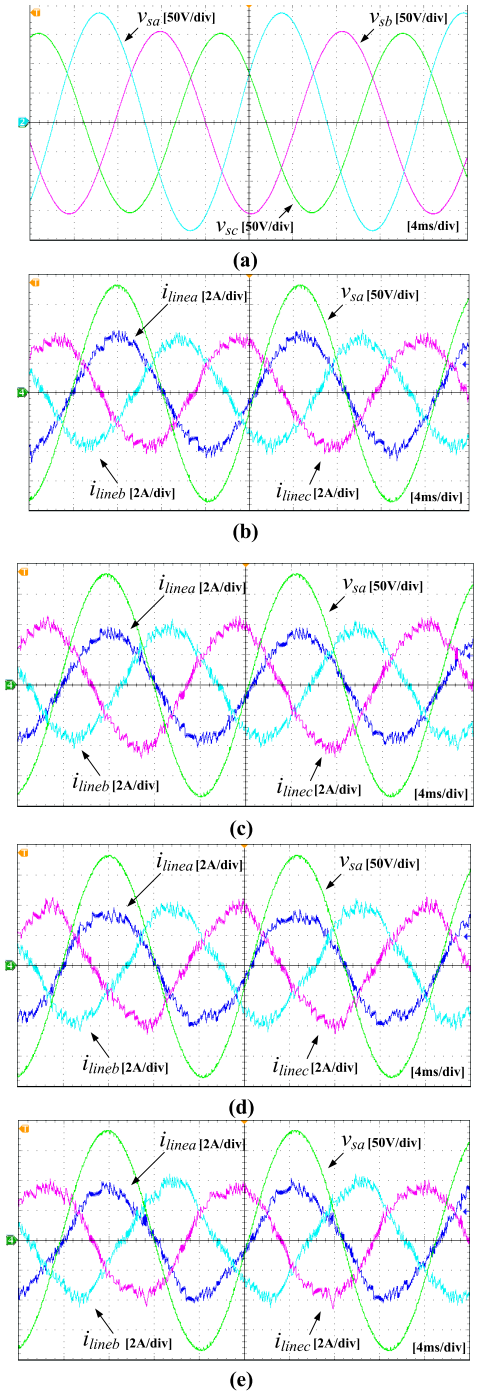

FIGURE 13. Experimental waveforms of three-phase line currents with imbalanced three-phase line voltages with *a*-phase source unbalanced by 20 percent ($\mu_a = 0.2$, $\mu_b = 0$ and $\mu_c = 0$) with (a) three-phase line voltage (b) MP-CC method (c) MP-VFC method (d) MP-DPC method, and (e) MP-VFDPC method.

The average THD values of the line currents produced by the four control methods when the three-phase source voltage was contaminated by the addition of the 5th harmonic component are shown in Fig. 8. The effects of the distorted input voltage on the THD values were similar to

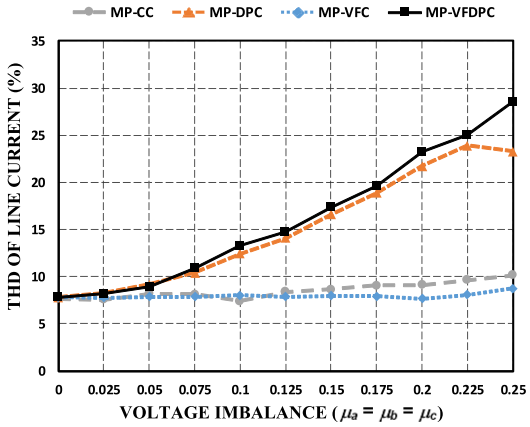

FIGURE 14. Average THD values of line currents resulting from four control methods under imbalanced supply voltages three-phase source unbalanced together ($\mu_a = \mu_b = \mu_c$, which vary from zero to 0.25).

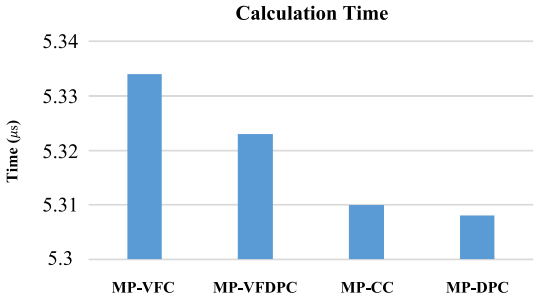

FIGURE 15. Computational effort.

those with *a*-phase supply voltage distortion with the 5th harmonic components in Fig. 6. The THD values of the line currents obtained by the MP-CC and the MP-DPC methods sharply increased along with the distortion in the three-phase line voltages. In addition, the line current THD values of the MP-CC and the MP-DPC methods were found to be more dependent on the input voltage distortion in the case of three-phase distortion than the *a*-phase supply voltage distortion in Fig. 6. However, the MP-VFC and MP-VFDPC methods produced much lower THD values than the other two methods, as shown in Fig. 8. Furthermore, the dependence of the three-phase voltage distortion on the line current THD values by the MP-VFC and MP-VFDPC methods was similar to that for the *a*-phase voltage distortion in Fig. 6.

The effects of a distorted supply voltage when the *a*-phase source was contaminated by the addition of the 7th harmonic component on the average THD values of the line currents is shown in Fig. 9. Mathematically, this distortion can be described as [12], [27], [28]:

$$\begin{aligned}
\mu v_{sa} &= V_m \sin(\omega t) + {}_{a7}V_m \sin(7\omega t) \\
\mu v_{sb} &= V_m \sin\left(\omega t - \frac{2}{3}\pi\right) + {}_{b7}V_m \sin\left(7\omega t - \frac{2}{3}\pi\right) \\
\mu v_{sc} &= V_m \sin\left(\omega t + \frac{2}{3}\pi\right) + {}_{c7}V_m \sin\left(7\omega t + \frac{2}{3}\pi\right), \quad (13)
\end{aligned}$$

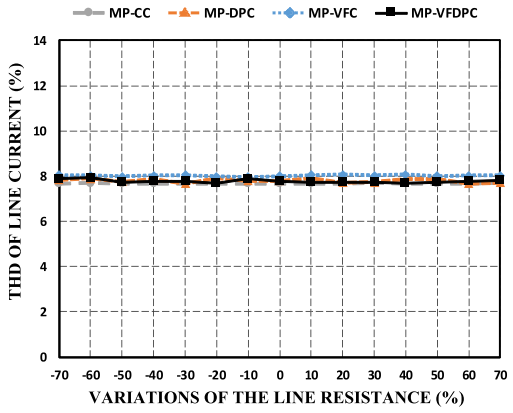

(a)

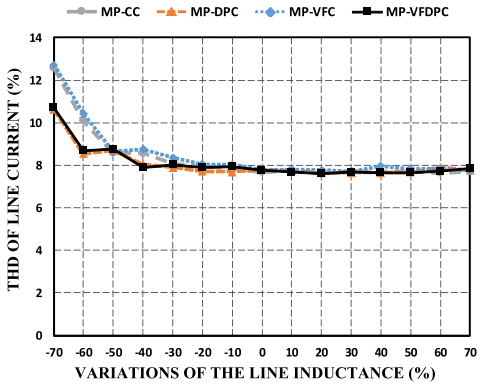

(b)

FIGURE 16. Line current THD values versus model errors in (a) line resistance (b) line inductance.

where, $\mu_{i7}(i = a, b, c)$ is the ratio between the magnitude of the 7th harmonic component and the magnitude of the fundamental component for each phase of the line voltage.

As was the case for the 5th harmonic distortion in Fig. 6, the MP-VFC and MP-VFDPC methods were found to be less affected by the addition of 7th harmonic distortion as both algorithms utilized the virtual fluxes as the control variables, which introduces a low-pass filter into the integrator. The experimental results for this test are shown in Fig. 10, where the a-phase source was contaminated by adding a 20% ($\mu_{a7} = 0.2$) magnitude 7th harmonic. The complete input waveform is shown in Fig. 10 (a), where it can be seen that the MP-VFC and MP-VFPDC methods produced line currents with lower harmonic distortion compared to those of the other methods despite the high degree of distortion applied to the input a-phase supply voltage waveform.

The average THD values of the line currents generated by the four algorithms when the three-phase sources were distorted by the addition of a 7th harmonic component are shown in Fig. 11. As shown, the trends in the THD values were similar to those when only the a-phase supply voltage was distorted, as shown in Fig. 9. However, the line current THD values of the MP-CC and MP-DPC methods were seen to be more highly dependent on the line voltage distortion

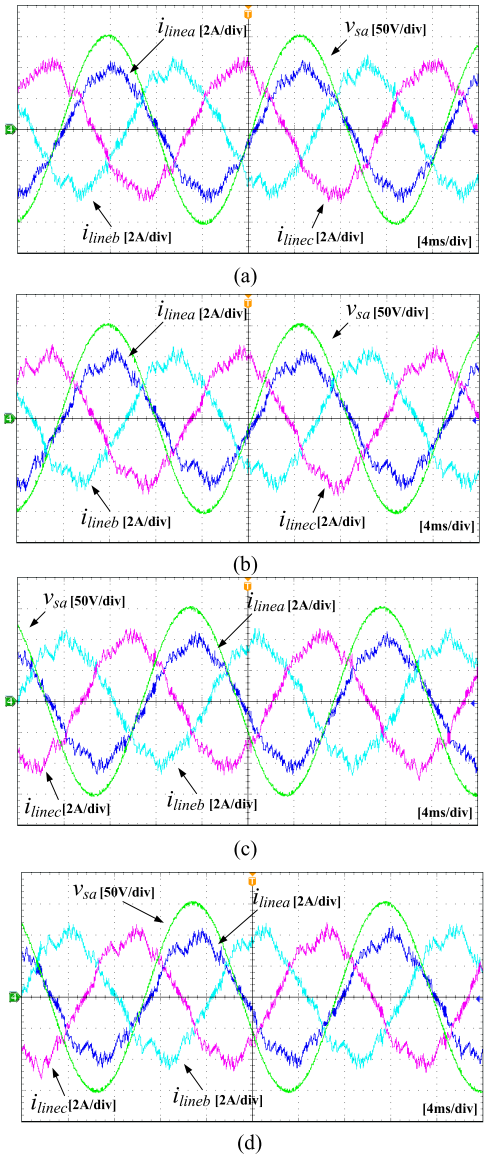

(a) (b) (c) (d)

FIGURE 17. Experimental waveforms of line currents with 50% underestimated inductance and exact resistance for (a) MP-CC (b) MP-VFC (c) MP-DPC and (d) MP-VFDPC methods.

in the case of the three-phase distortion as compared to the results of the a-phase only supply voltage distortion in Fig. 9.

B. EFFECT OF UNBALANCED LINE VOLTAGES

The THD values of the line currents obtained by the four control methods with unbalanced line voltages were also investigated. The unbalanced line voltages can be represented by [12], [27], [29]:

$$\begin{aligned}
\mu v_{sa} &= V_m \sin(\omega t) + {}_a V_m \sin(\omega t) \\
\mu v_{sb} &= V_m \sin\left(\omega t - \frac{2}{3}\pi\right) + {}_b V_m \sin\left(\omega t + \frac{2}{3}\pi\right) \\
\mu v_{sc} &= V_m \sin\left(\omega t + \frac{2}{3}\pi\right) + {}_c V_m \sin\left(\omega t - \frac{2}{3}\pi\right), \quad (14)
\end{aligned}$$

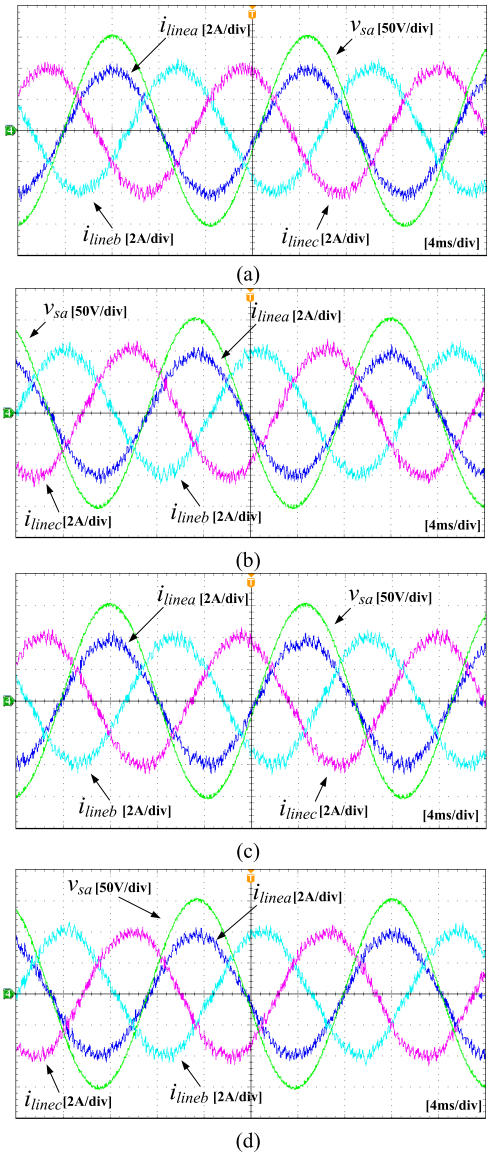

FIGURE 18. Experimental waveforms of line currents with 50% overestimated inductance and exact resistance for (a) MP-CC (b) MP-VFC (c) MP-DPC and (d) MP-VFDPC methods.

where $\mu_i (i = a, b, c)$ is the ratio between the magnitudes of the unbalanced term for each phase of the line voltage. The corresponding THD values of the line currents obtained by the four methods are shown in Fig. 12.

As shown in Fig. 12, for an unbalanced a-phase supply voltage, it was found that the MP-DPC and MP-VFDPC methods, which used the input power components as the control variables, generated more harmonics in the line currents than the MP-CC and the MP-VFC methods. The results for an unbalanced three-phase voltage source in which the a-phase source voltage was unbalanced by 20% are shown in Fig. 13 (a) shows the input three-phase voltage waveform while parts (b), (c), (d), and (e) show the results for the MP-CC, MP-VFC, MP-DPC, and MP-VFDPC methods, respectively. As shown, the MP-DPC and MP-VFDPC methods generated more highly distorted current waveforms

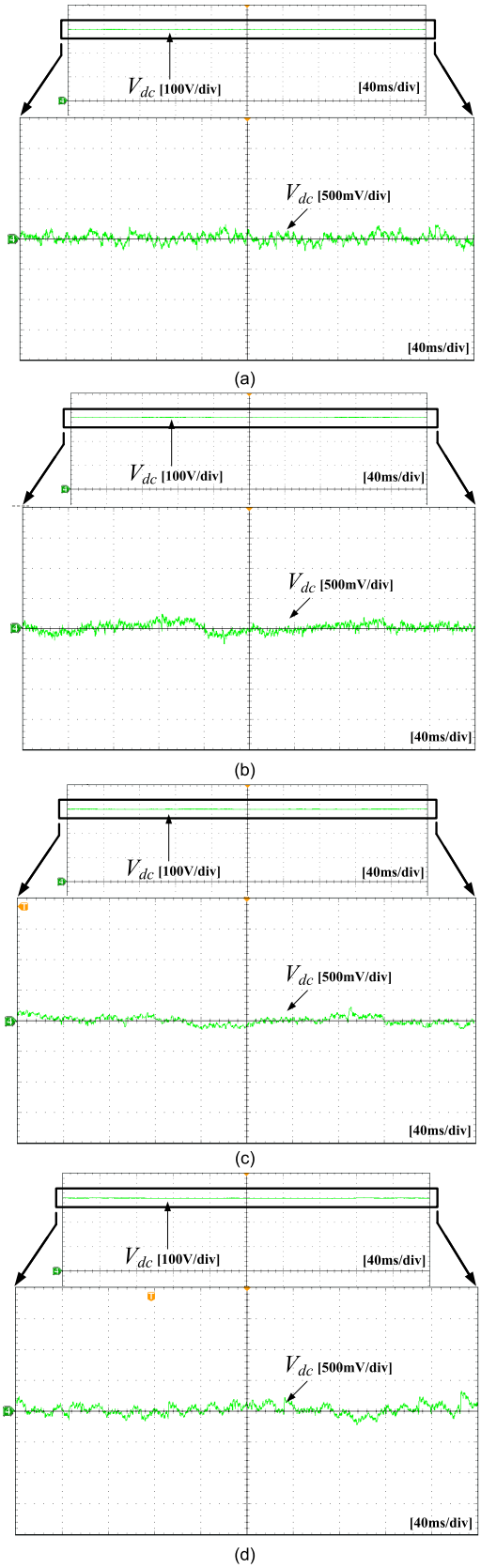

FIGURE 19. Experimental waveforms of the output voltage waveforms and their ac ripple components with no line voltage distortion obtained with (a) MPCC method (b) MP-VFC method (c) MP-DPC method, and (d) MP-VFDPC method.

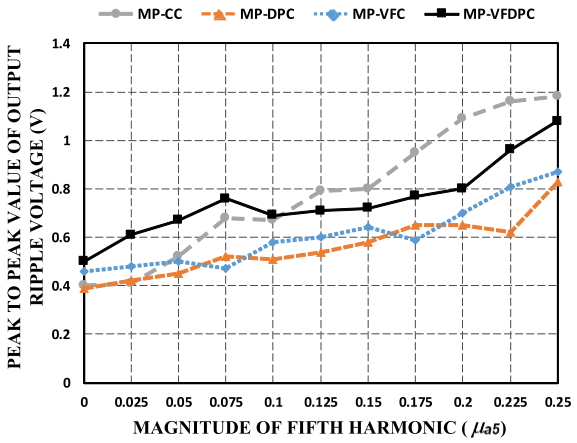

FIGURE 20. Peak-to-peak values of output ripple voltages resulting from four control methods under distorted line voltage with *a*-phase line voltage contaminated with 5th harmonics (μ_{a5} varying from zero to 0.25, $\mu_{b5} = 0$ and $\mu_{c5} = 0$).

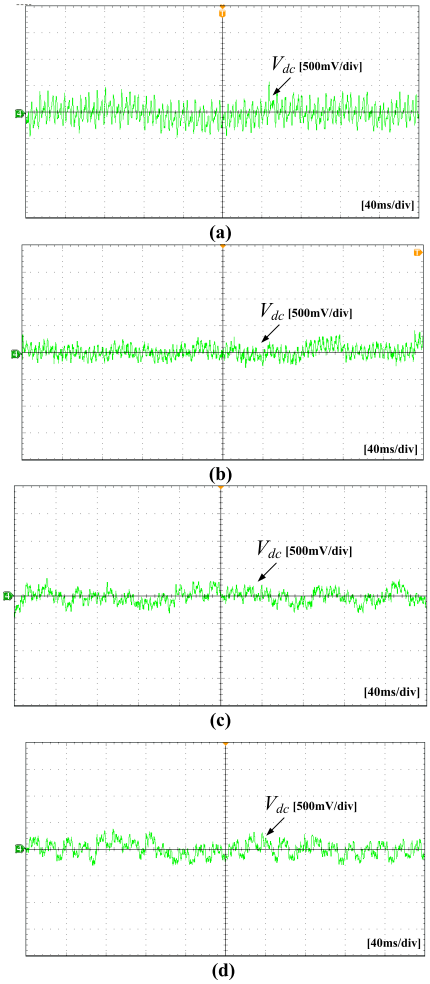

FIGURE 21. Experimental waveforms of ac ripple components of the output voltage under distorted line voltage with *a*-phase source contaminated with 5th harmonics by 20 percent ($\mu_{a5} = 0.2$, $\mu_{b5} = 0$ and $\mu_{c5} = 0$) with (a) MPCC method (b) MP-VFC method (c) MP-DPC method, and (d) MP-VFDPC method.

with higher THD values than the MP-CC and MP-VFC methods.

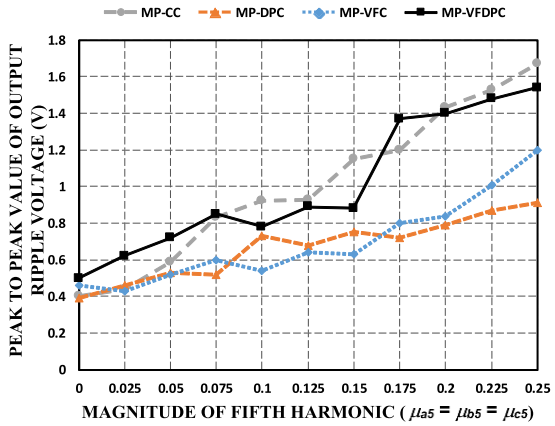

FIGURE 22. Peak-to-peak values of output ripple voltages resulting from four control methods under distorted line voltage with three-phase sources contaminated with 5th harmonics ($\mu_{a5} = \mu_{b5} = \mu_{c5}$, which vary from zero to 0.25).

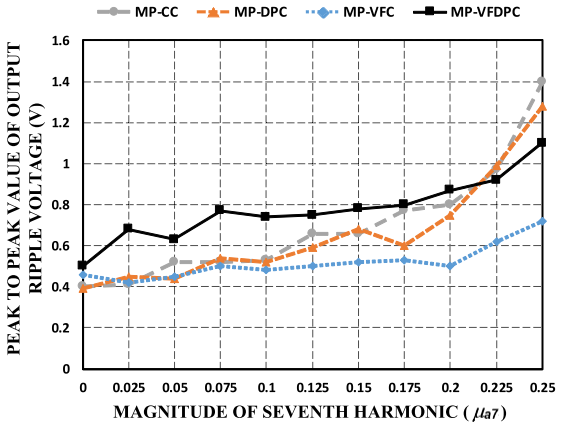

FIGURE 23. Peak-to-peak values of output ripple voltages resulting from four control methods under distorted line voltage with *a*-phase line voltage contaminated with 7th harmonics (μ_{a7} varying from zero to 0.25, $\mu_{b7} = 0$ and $\mu_{c7} = 0$).

The average THD values of the line currents resulting from the four control methods for an unbalanced three-phase input voltage are shown in Fig. 14. The trends observed in this figure are similar to those for the unbalanced *a*-phase supply voltage in Fig. 12. The MP-DPC and MP-VFDPC methods, which are based on the direct power control method generated THD values that increased markedly as the imbalance in the three-phase line voltages increased. Moreover, the THD values of the MP-DPC and MP-VFDPC methods were found to be more highly dependent on the line voltage unbalance in the case of a three-phase supply versus the *a*-phase supply voltage unbalance in Fig. 12. By contrast, the MP-CC and MP-VFC methods generated much lower THD values than the other two methods, as shown in Fig. 14.

C. COMPLEXITY OF THE CONTROL ALGORITHMS

Each of the four algorithms differ in terms of the complexity when implemented in a digital signal processor (DSP). The execution time for each of the algorithms was computed by

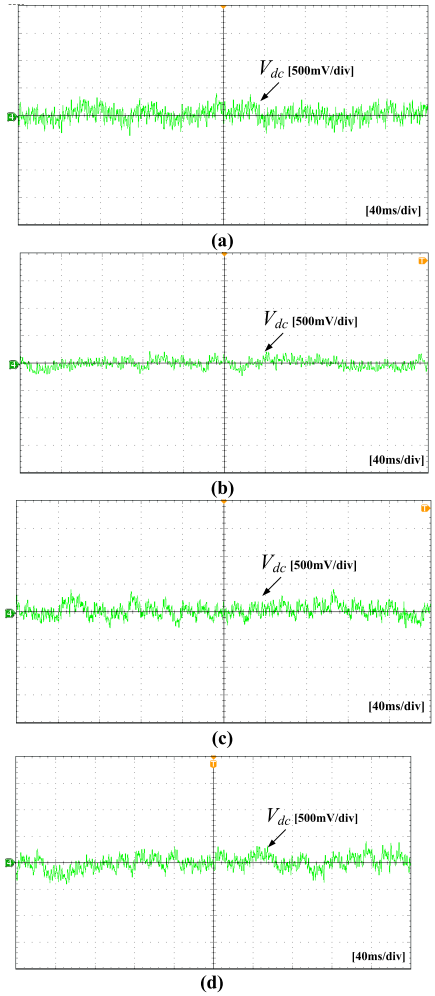

FIGURE 24. Experimental waveforms of ac ripple components of the output voltage under distorted line voltage with *a*-phase source contaminated with 7th harmonics by 20 percent ($\mu_{a7} = 0.2$, $\mu_{b7} = 0$ and $\mu_{c7} = 0$) with (a) MPCC method (b) MP-VFC method (c) MP-DPC method, and (d) MP-VFDPC method.

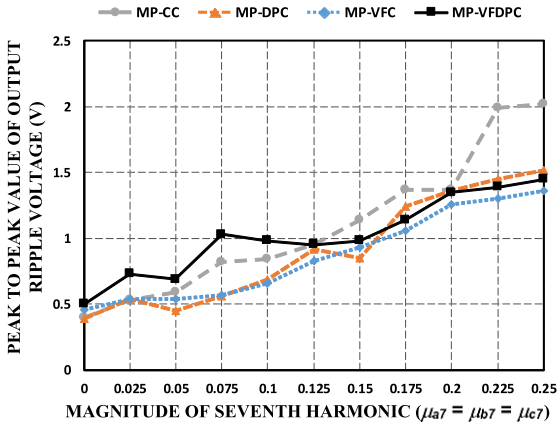

FIGURE 25. Peak-to-peak values of output ripple voltages resulting from four control methods under distorted line voltage with three-phase sources contaminated with 7th harmonics ($\mu_{a7} = \mu_{b7} = \mu_{c7}$, which vary from zero to 0.25).

measuring the elapsed time in the experimental setup, and the results are shown in Fig. 15. In the figure, it can be seen that

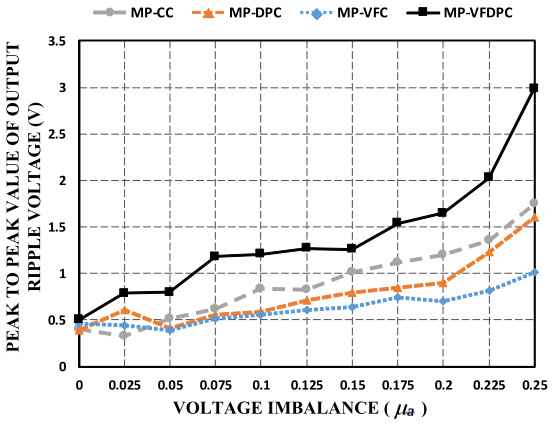

FIGURE 26. Peak-to-peak values of output ripple voltages resulting from four control methods with *a*-phase source unbalanced (μ_a varying from zero to 0.25, $\mu_b = 0$, and $\mu_c = 0$).

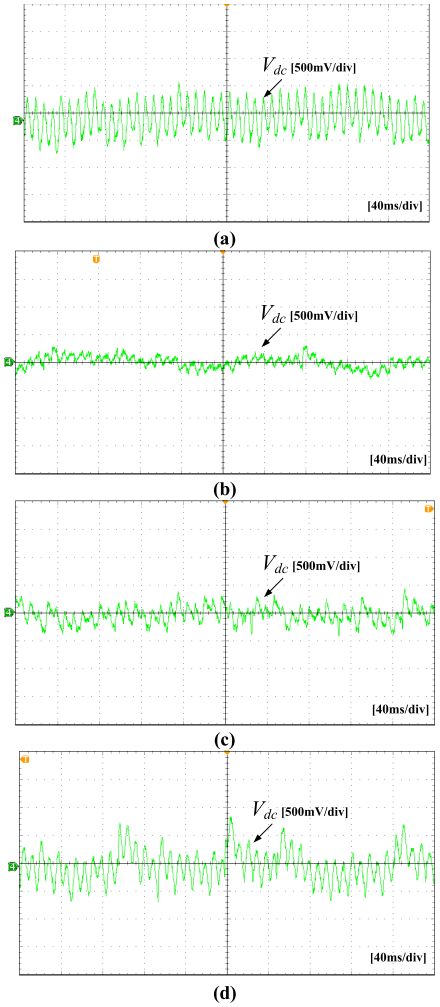

FIGURE 27. Experimental waveforms of ac ripple components of the output voltage with imbalanced three-phase line voltages with *a*-phase source unbalanced by 20 percent ($\mu_a = 0.2$, $\mu_b = 0$ and $\mu_c = 0$) with (a) MPCC method (b) MP-VFC method (c) MP-DPC method, and (d) MP-VFDPC method.

the MP-VFC and MP-VFDPC methods, which were based on the virtual flux, required more execution time than the others.

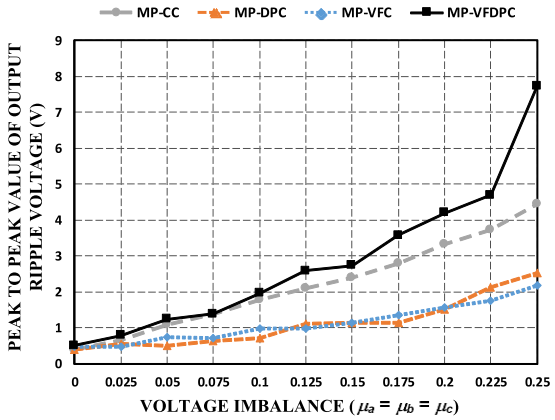

FIGURE 28. Peak-to-peak values of output ripple voltages resulting from four control methods with three-phase source unbalanced together ($\mu_a = \mu_b = \mu_c$, which vary from zero to 0.25).

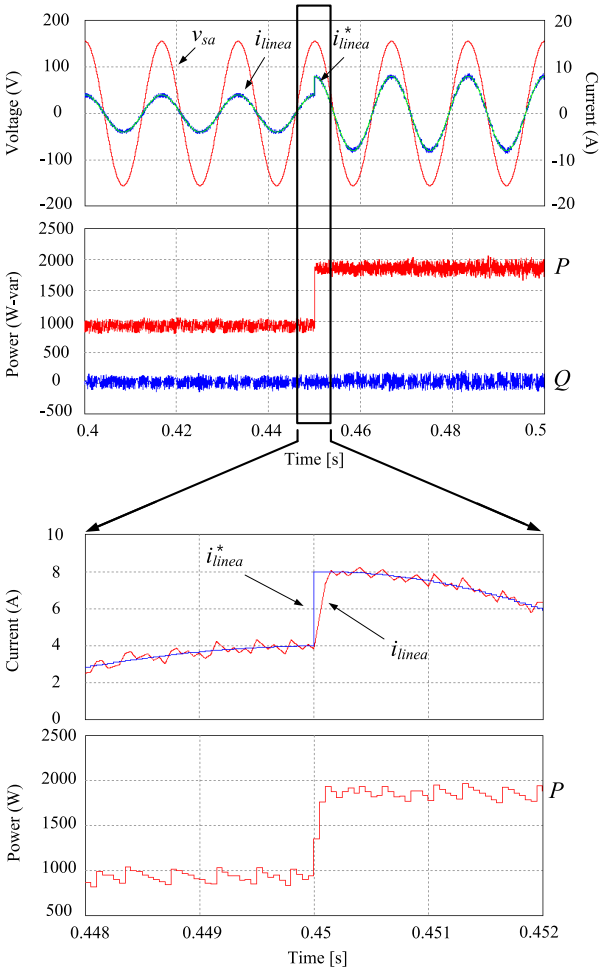

FIGURE 29. Simulated response of MP-CC method with step-change of line current reference from 4 A to 8 A.

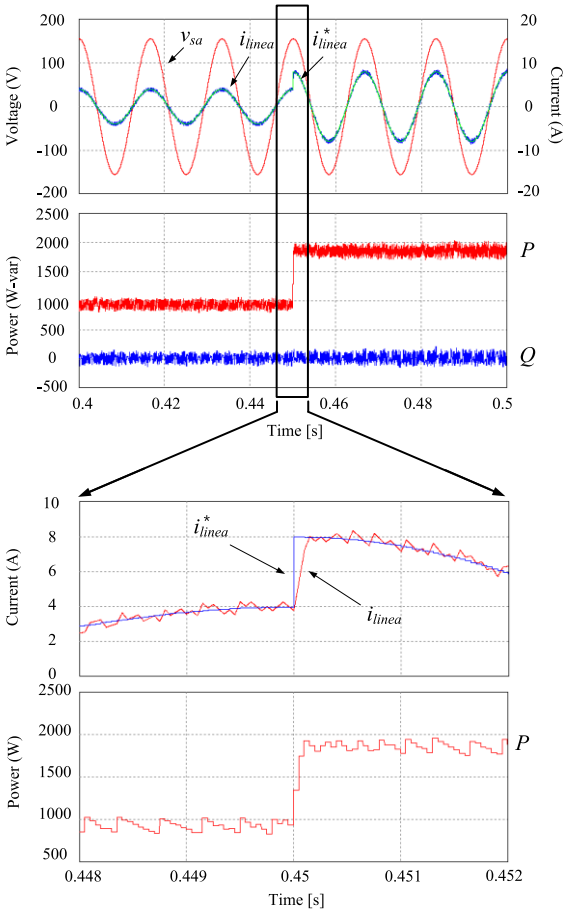

FIGURE 30. Simulated response of MP-VFC method with step-change.

D. SENSITIVITY TO MODEL ERRORS

All four control methods incorporated the line resistance and inductance as parameters, and all were based on the model predictive control algorithm. In addition, the performance of an AFE rectifier operated with the four control methods was affected by the model accuracy. The effects of errors in the line resistance and inductance on the THD values of the line currents obtained from the four control methods are compared in Fig. 16, and it can be seen that the trends in the effects of the error on the quality for each model were similar. Errors in the line resistance had little effect on the quality of the line current. In contrast, the current THD values were seen to be more affected by the line inductance than by the line resistance in all four control schemes. In particular, underestimations in the line inductance were found to seriously degrade the performance of the AFE rectifiers for all control methods. On the other hand, the effects of an overestimation of the inductance on the THD values of the four methods were found to be negligible.

The effects of inductance errors on the performance of the control models are compared in Figs. 17 and 18. The results of the case where the control algorithms were operated with a 50% underestimated inductance and exact resistance are shown in Fig. 17. In this figure, it can be seen that the line currents of all methods exhibited increased distortion. The waveforms for the case where the inductance was overestimated by 50% and the resistance was correct are shown in

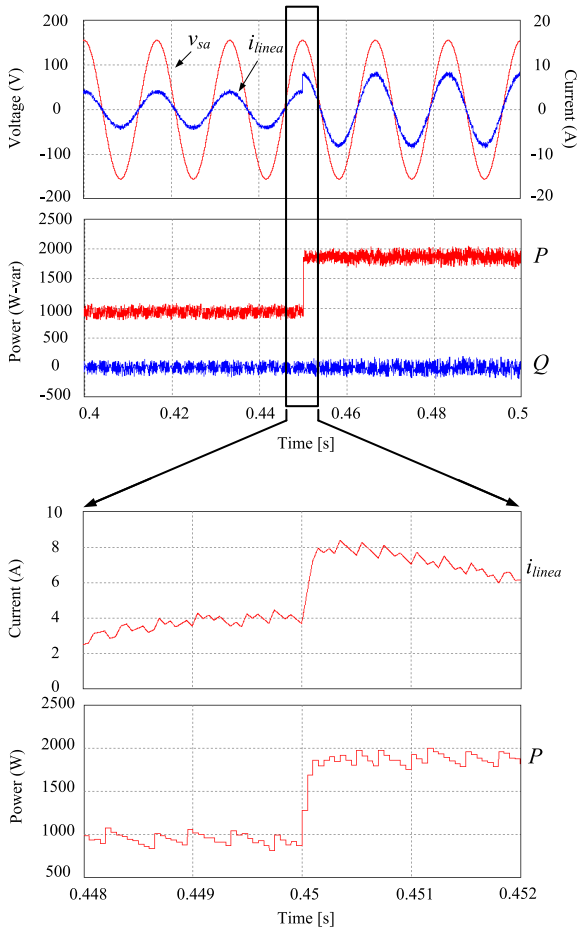

FIGURE 31. Simulated response of MP-DPC method with step-change.

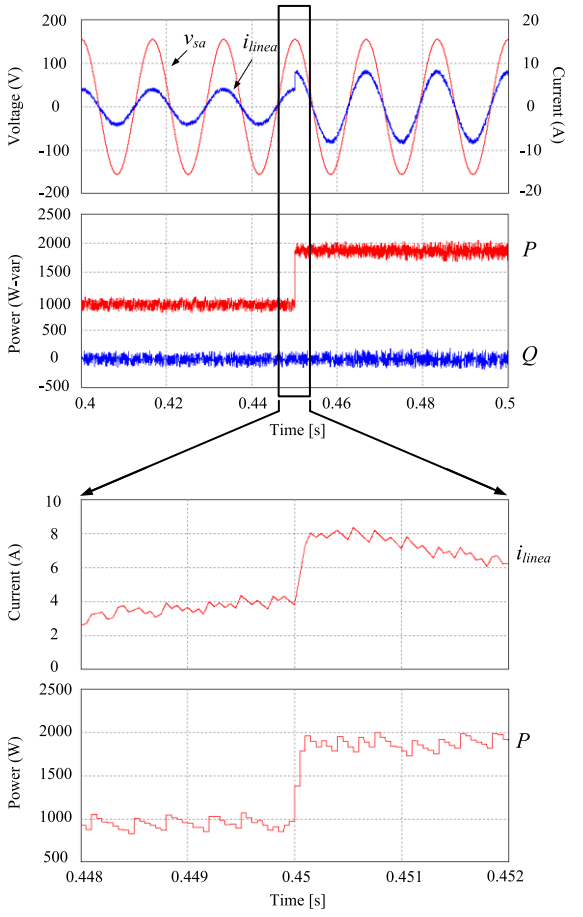

FIGURE 32. Simulated response of MP-VFDPC method with step-change.

Fig. 18. As shown, the current waveforms for this case were less distorted than those with the underestimated inductance in Fig. 17.

E. OUTPUT VOLTAGE QUALITY

The output voltage quality obtained by the four control methods was investigated and included in the revised paper, because the output voltage quality is an important factor to evaluate the performance of the AFE rectifiers. Fig. 19 illustrates the experimental results of the output voltage waveform V_{dc} in the AFE rectifier obtained by the four control methods with balanced supply voltages with no distortion. It should be noted that ac component waveforms of the output voltage V_{dc} are displayed with expanded waveform to more clearly show differences in ripples contained in the output voltage waveforms. It is seen from Fig. 19 that the output voltages produced in the rectifiers operated by the four control are well regulated whereas the ripple waveforms look a little different.

Fig. 20 shows the peak-to-peak values of the output ripple voltages resulting from the four control methods with distorted line voltages, where the *a*-phase line voltage was contaminated by the addition of the 5th harmonic component while no harmonic components were added to the *b*- and *c*-phases. It can be seen in Fig. 20 that as the magnitude of μ_{a5} increased, the peak-to-peak output ripple voltages of the four methods increased. The MP-CC and MP-VFDPC methods produced slightly higher ripple values on conditions of higher distortions than the MP-VFC and MP-DPC methods. The experimental results of the ac components of the output voltage waveforms obtained via the four control methods for a distorted line voltage are shown in Fig. 21.

The peak-to-peak values of the output ripple voltages produced by the four control methods when the three-phase source voltage was contaminated by the addition of the 5th harmonic component are shown in Fig. 22. As expected, the ripples increase as increasing distortion of the supply voltages. In addition, the effects of the distorted input voltage on the THD values were similar to those with *a*-phase supply voltage distortion with the 5th harmonic components in Fig. 20. However, the ripples resulted from three-phase distortions in Fig. 22 are bigger than those obtained by *a*-phase supply voltage distortion in Fig. 20. It is also expected that the output voltage ripples more sharply increase with lower dc capacitance.

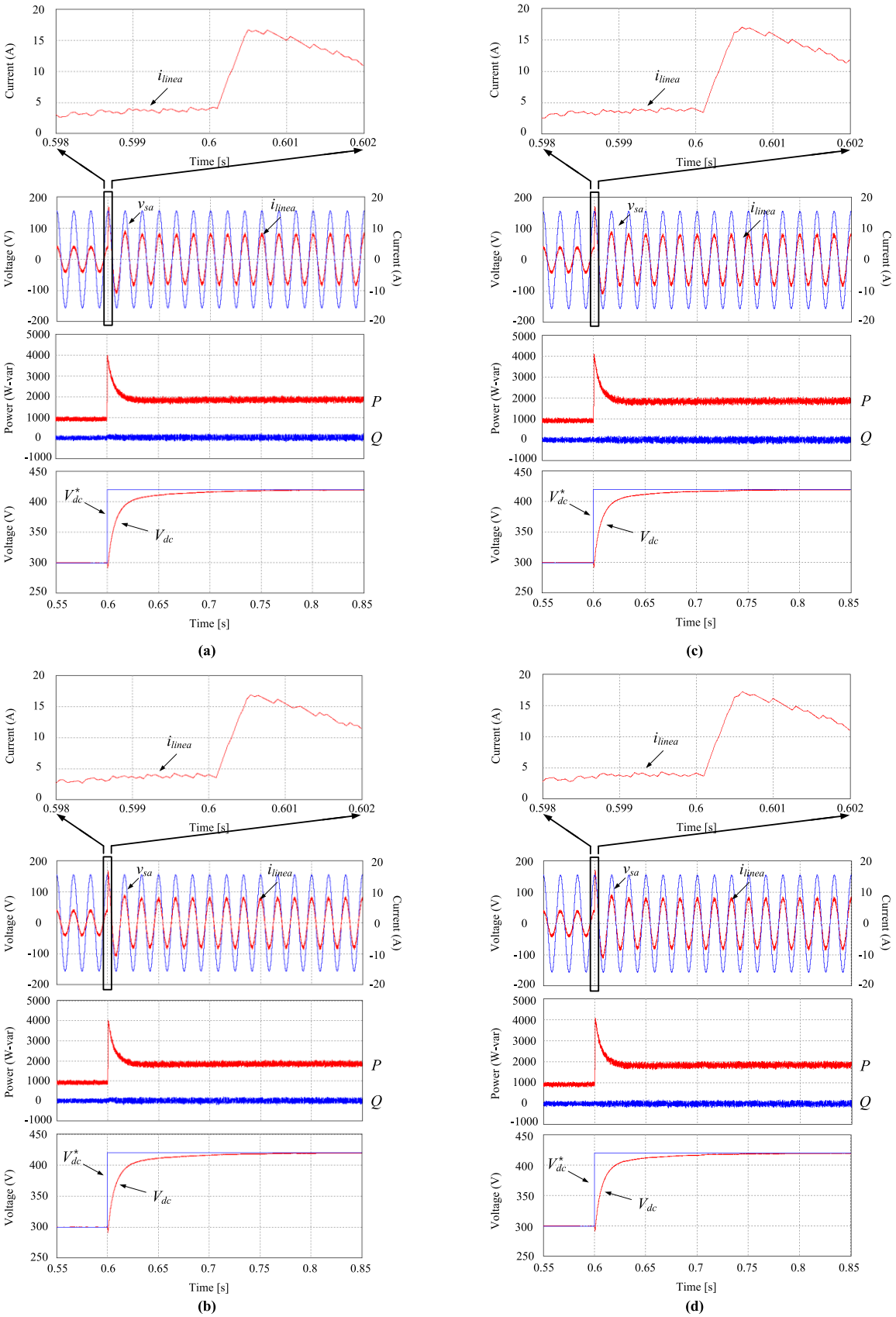

FIGURE 33. Simulated response of with step-change of dc voltage reference from 300 V to 425 V with (a) MPCC method (b) MP-VFC method (c) MP-DPC method, and (d) MP-VFDPC method.

Fig. 23 shows the peak-to-peak values of the output ripple voltages resulting from the four control methods with distorted line voltages, where the *a*-phase line voltage was contaminated by the addition of the 7th harmonic component while no harmonic components were added to the *b*- and *c*-phases. It can be seen in Fig. 23 that as the magnitude of μ_{a7} increased, the peak-to-peak output ripple voltages of the four methods increased. The experimental results of the ac components of the output voltage waveforms obtained via the four control methods for a distorted line voltage are shown in Fig. 24. The peak-to-peak values of the output ripple voltages produced by the four control methods when the three-phase source voltage was contaminated by the addition of the 7th harmonic component are shown in Fig. 25.

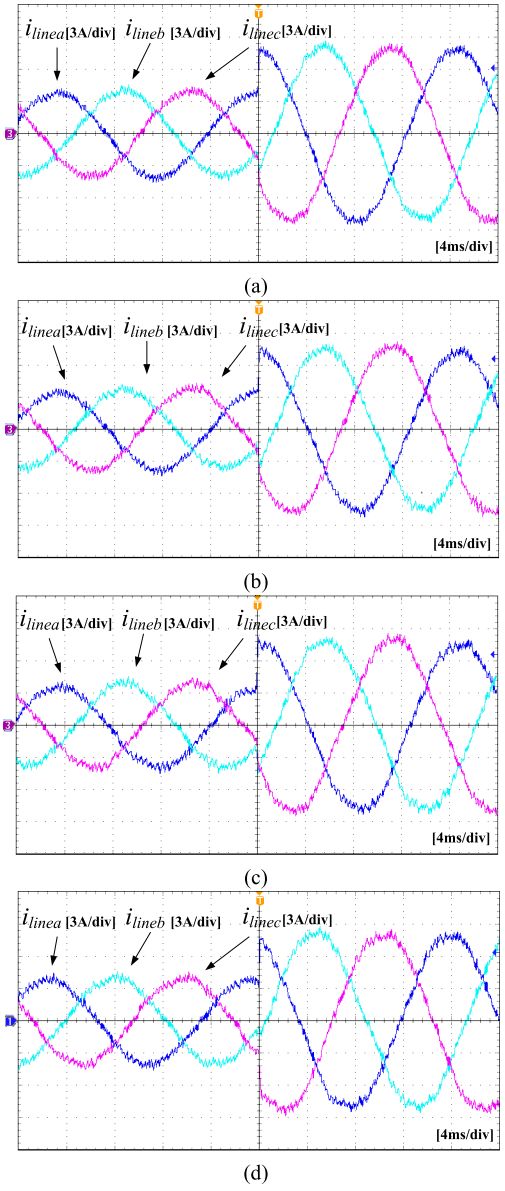

FIGURE 34. Line current waveforms for transient response by (a) MP-CC (b) MP-VFC (c) MP-DPC and (d) MP-VFDPC methods.

Fig. 26 shows the peak-to-peak values of the output ripple voltages resulting from the four control methods with an unbalanced *a*-phase supply voltage. The experimental results of the ac components of the output voltage waveforms obtained via the four control methods with an unbalanced *a*-phase supply voltage are shown in Fig. 27. The peak-to-peak values of the output ripple voltages produced by the four control methods with an unbalanced three-phase supply voltage are shown in Fig. 28. From Figs. 26 and 28, it is clearly shown that the peak-to-peak output ripple voltages of the four methods increase as the supply voltage is more severely distorted.

F. DYNAMIC PERFORMANCE

The dynamic response of the four control methods were investigated under the same transient conditions. The effects of the PI control block used for dc output voltage regulation on the rectifier dynamic performances were ignored, by directly making manual step-changes of the current reference and the other control variables, in order to focus on the performance differences between the respective model predictive control methods. Simulated waveforms depicting a step change in an AFE rectifier operated by the MP-CC method are shown in Fig. 29. In this case, the reference line current used as the control variable changed abruptly from 4 to 8 A. The simulation results of the other three control methods for the same magnitude step change are illustrated in Figs. 30 to 32, in which the respective control variable references of the three methods are set to experience step changes corresponding to the same amount as the MP-CC method. From these figures, it can be seen that the four control methods all exhibited fast dynamic responses despite differences in their control variables and control structures. This is because all were based on the same model predictive control platform, which has fast dynamic characteristics.

TABLE 1. Summary of performance comparisons.

Performance	Control methods			
	MP-CC	MP-VFC	MP-DPC	MP-VFDPC
Robustness to 5^{th} and 7^{th} line voltage harmonics	normal	excellent	normal	excellent
Robustness to line voltage unbalance	excellent	excellent	normal	normal
Effects of input inductance mismatch	small	small	small	small
Effects of input resistance mismatch	negligible	negligible	negligible	negligible
Output voltage quality against line voltage harmonics and unbalance	normal	good	normal	normal
Calculation burden	low	highest	lowest	high
Dynamic response	fast	fast	fast	fast

The dynamic responses of the four methods by making step-changes of the voltage references, in which transient performance includes the PI controllers in addition to the model predictive control method, are also investigated in Fig. 33. The reference values of the dc voltage were forced to change from 300 V to 425 V suddenly, for all the four control methods. It was proved that the four model predictive control methods showed almost same fast dynamic responses even including the PI controllers from Fig. 33.

The experimental dynamic response of the four control methods are shown in Fig. 34 for the same magnitude of step change as that used in the simulations. As shown, the response times of all four control methods to the same step input were almost the same. Table 1 shows a summary of comparative results of the four control methods.

IV. CONCLUSION

In this paper, the relative performance of four model predictive control algorithms were compared in terms of the quality of the produced line current under a variety of adverse conditions, such as an unbalanced input voltage, distorted input voltage, and uncertainty in the parameters. The theoretical background of the control methods was presented, followed by the results of both simulation and experiment. With regard to the line current quality for input line voltages distorted by the addition of 5^{th} or 7^{th} order harmonics components, the control methods that were based on the virtual flux, i.e., the MP-VFC and MP-VFDPC methods, exhibited marked advantages over the MP-CC and MP-DPC methods. However, the MP-VFC and MP-VFDPC methods were found to be more computationally complex than the others. It was also found that when the AFE rectifier received an unbalanced line voltage, the MP-CC and MP-VFC methods produced a better line current harmonic spectrum than that produced by the other methods. It was also determined that the four methods had little difference in their dynamic performance and parameter sensitivity. In summary, based on the results of this study, the MP-VFC scheme was found to be distinctly superior to the other three schemes for distorted and unbalanced line voltages.

REFERENCES

[1] J. R. Rodriguez, J. W. Dixon, J. R. Espinoza, J. Pontt, and P. Lezana, "PWM regenerative rectifiers: State of the art," *IEEE Trans. Ind. Electron.*, vol. 52, no. 1, pp. 5–22, Feb. 2005.

[2] M. P. Kazmierkowski, R. Krishnan, and F. Blaabjerg, *Control in Power Electronics*. New York, NY, USA: Academic, 2002.

[3] T. Noguchi, H. Tomiki, S. Kondo, and I. Takahashi, "Direct power control of PWM converter without power-source voltage sensors," *IEEE Trans. Ind. Appl.*, vol. 34, no. 3, pp. 473–479, May 1998.

[4] S. Vazquez, J. A. Sanchez, J. M. Carrasco, J. I. Leon, and E. Galvan, "A model-based direct power control for three-phase power converters," *IEEE Trans. Ind. Electron.*, vol. 55, no. 4, pp. 1647–1657, Apr. 2008.

[5] M. Malinowski, M. Jasinski, and M. P. Kazmierkowski, "Simple direct power control of three-phase PWM rectifier using space-vector modulation (DPC-SVM)," *IEEE Trans. Ind. Electron.*, vol. 51, no. 2, pp. 447–454, Apr. 2004.

[6] A. Bouafia, J.-P. Gaubert, and F. Krim, "Predictive direct power control of three-phase pulsewidth modulation (PWM) rectifier using space-vector modulation (SVM)," *IEEE Trans. Power Electron.*, vol. 25, no. 1, pp. 228–236, Jan. 2010.

[7] C. Lascu, I. Boldea, and F. Blaabjerg, "A modified direct torque control for induction motor sensorless drive," *IEEE Trans. Ind. Appl.*, vol. 36, no. 1, pp. 122–130, Jan. 2000.

[8] A. Bouafia, F. Krim, and J. P. Gaubert, "Fuzzy-logic-based switching state selection for direct power control of three-phase PWM rectifier," *IEEE Trans. Ind. Electron.*, vol. 56, no. 6, pp. 1984–1992, Jun. 2009.

[9] J. Hu, L. Shang, Y. He, and Z. Q. Zhu, "Direct active and reactive power regulation of grid-connected DC/AC converters using sliding mode control approach," *IEEE Trans. Power Electron.*, vol. 26, no. 1, pp. 210–222, Jan. 2011.

[10] J. Rodríguez *et al.*, "State of the art of finite control set model predictive control in power electronics," *IEEE Trans. Ind. Informat.*, vol. 9, no. 2, pp. 1003–1016, May 2013.

[11] I. S. Mohamed, S. A. Zaid, M. F. Abu-Elyazeed, and H. M. Elsayed, "Implementation of model predictive control for three-phase inverter with output LC filter on eZdsp F28335 Kit using HIL simulation," *Int. J. Model. Identificat. Control*, vol. 25, no. 4, pp. 301–312, 2016.

[12] M. Malinowski, M. P. Kazmierkowski, and A. M. Trzynadlowski, "A comparative study of control techniques for PWM rectifiers in AC adjustable speed drives," *IEEE Trans. Power Electron.*, vol. 18, no. 6, pp. 1390–1396, Nov. 2003.

[13] J. Rodríguez *et al.*, "Predictive current control of a voltage source inverter," *IEEE Trans. Ind. Electron.*, vol. 54, no. 1, pp. 495–503, Feb. 2007.

[14] P. Cortes, J. Rodriguez, C. Silva, and A. Flores, "Delay compensation in model predictive current control of a three-phase inverter," *IEEE Trans. Ind. Electron.*, vol. 59, no. 2, pp. 1323–1325, Feb. 2012.

[15] J.-C. Kim and S. Kwak, "Model predictive virtual flux control to improve performance under distorted input voltage conditions," *IEEE Trans. Access*, vol. 6, pp. 34921–34933, Jun. 2018.

[16] S. Kwak, S.-J. Yoo, and J. Park, "Finite control set predictive control based on Lyapunov function for three-phase voltage source inverters," *IET Power Electron.*, vol. 7, no. 11, pp. 2726–2732, 2014.

[17] D.-K. Choi and K.-B. Lee, "Dynamic performance improvement of AC/DC converter using model predictive direct power control with finite control set," *IEEE Trans. Ind. Electron.*, vol. 62, no. 2, pp. 757–767, Feb. 2015.

[18] S. Kwak and J. C. Park, "Model-predictive direct power control with vector preselection technique for highly efficient active rectifiers," *IEEE Trans Ind. Informat.*, vol. 11, no. 1, pp. 44–52, Feb. 2015.

[19] M. Malinowski, M. P. Kazmierkowski, S. Hansen, F. Blaabjerg, and G. D. Marques, "Virtual-flux-based direct power control of three-phase PWM rectifiers," *IEEE Trans. Ind. Appl.*, vol. 37, no. 4, pp. 1019–1027, Jul./Aug. 2001.

[20] Y. Cho and K.-B. Lee, "Virtual-flux-based predictive direct power control of three-phase PWM rectifiers with fast dynamic response," *IEEE Trans. Power Electron.*, vol. 31, no. 4, pp. 3348–3359, Apr. 2016.

[21] P. Antoniewicz and M. P. Kazmierkowski, "Virtual-flux-based predictive direct power control of AC/DC converters with online inductance estimation," *IEEE Trans. Ind. Electron.*, vol. 55, no. 12, pp. 4381–4390, Dec. 2008.

[22] M. Hosein and S. A. Davari, "Virtual flux model predictive direct power control (VF-MPDPC) of AFE rectifier with new current prediction method and negative sequence elimination," in *Proc. IEEE Int. Symp. PRECEDE*, Sep. 2017, pp. 113–118.

[23] J. L. Duarte, A. V. Zwam, C. Wijnands, and A. Vandenput, "Reference frames fit for controlling PWM rectifiers," *IEEE Trans. Ind. Electron.*, vol. 46, no. 3, pp. 628–630, Jun. 1999.

[24] J. Rodriguez and P. Cortes, *Predictive Control of Power Converters and Electrical Drives*. New York, NY, USA: Wiley, 2012, pp. 31–39.

[25] Y. Tao, Q. Wu, L. Wang, and W. Tang, "Voltage sensorless predictive direct power control of three-phase PWM converters," *IET Power Electron.*, vol. 9, no. 5, pp. 1009–1018, Apr. 2016.

[26] S. Kwak and J.-C. Park, "Predictive control method with future zero-sequence voltage to reduce switching losses in three-phase voltage source inverters," *IEEE Trans. Power Electron.*, vol. 30, no. 3, pp. 1558–1566, Mar. 2015.

[27] B. Liu, F. Zhuo, Y. Zhu, H. Yi, and F. Wang, "A three-phase PLL algorithm based on signal reforming under distorted grid conditions," *IEEE Trans. Power Electron.*, vol. 30, no. 9, pp. 5272–5283, Sep. 2015.
[28] T. R. Kuphaldt, *Lessons in Electric Circuits*, vol. 2, 6th ed. Design Science License, 2007.
[29] P. Pillay, P. Hofmann, and M. Manyage, "Derating of induction motors operating with a combination of unbalanced voltages and over or under-voltages," *IEEE Trans. Energy Convers.*, vol. 17, no. 4, pp. 485–491, Dec. 2002.

EUN-SU JUN received the B.S. degree from the School of Electronics Engineering, Kyungpook National University, Daegu, South Korea, in 2018. He is currently pursuing the M.S. degree in electrical and electronics engineering with Chung-Ang University, Seoul, South Korea. His research interests are control and analysis for power converters.

SANGSHIN KWAK (S'02–M'05) received the Ph.D. degree in electrical engineering from Texas A&M University, College Station, TX, USA, in 2005. From 1999 to 2000, he was a Research Engineer at LG Electronics, Changwon, South Korea. He was also with the Whirlpool R&D Center, Benton Harbor, MI, USA, in 2004. From 2005 to 2007, he was a Senior Engineer with the Samsung SDI R&D Center, Yongin, South Korea. From 2007 to 2010, he was an Assistant Professor at Daegu University, Gyeongsan, South Korea. Since 2010, he has been with Chung-Ang University, Seoul, South Korea, where he is currently a Professor. His research interests are topology design, modeling, modulation, and control of power converters, multilevel converters, renewable energy systems, and power quality.

TAEHYUNG KIM (M'04–SM'12) received the Ph.D. degree in electrical engineering from Texas A&M University, College Station, TX, USA, in 2003. He was with the Samsung Electronics' Digital Appliances Research Center as a Senior Research Engineer in 2003. From 2004 to 2005, he was a Post-Doctoral Researcher with the Advanced Vehicle, Power Electronics, and Motor Drive Laboratory, Texas A&M University. In 2005, he joined the Department of Electrical and Computer Engineering, University of Michigan–Dearborn, where he is currently an Associate Professor. In 2014, he visited Chung-Ang University as an invited Brain-Pool Research Scholar. His research interests include electric and hybrid electric vehicles, power electronics, and motor drives. He was a recipient of the 2012 Second Prize Paper Award from the IEEE Industry Applications Society (Annual Society's Best Magazine Article).